Flavin-enabled Oxidative C-C Bond Cleavage and Rearrangement Reactions in the Biosynthesis of Novel Oxaspiro Angucycline Derivatives

Guojian Zhang
Ocean University of China
Xiao Xu
Ocean University of China
Yimin Chang
Ocean University of China
Yinghan Chen
Ocean University of China
Luning Zhou
Ocean University of China
Falei Zhang
Ocean University of China
Chuanteng Ma
Ocean University of China
Qian Che
Ocean University of China
Blaine Pfeifer
University at Buffalo, State University of New York https://orcid.org/0000-0002-9338-2794
Tianjiao Zhu
Ocean University of China
Dehai Li (dehaili@ouc.edu.cn)
Ocean University of China https://orcid.org/0000-0002-7191-2002

Article

Keywords:

Posted Date: September 22nd, 2022

DOI: https://doi.org/10.21203/rs.3.rs-2066606/v1

Abstract

Flavin-enabled oxidative C-C Bond cleavages lead to fantastic structural alternations and are crucial for biological activity of many natural products. Here we report the discovery of novel atypical agucycline derivatives including spirocyclione A (1) which contains an unusual oxaspiro[5.5]undecane architecture and spirocyclione B (2) possessing an intriguing di-carboxylic substituted benzochromene scaffold by heterologous expression of a type II polyketide biosynthetic gene cluster. Biosynthesis studies demonstrated 1 and 2 are generated by sequential flavin-enabled C-C bond cleavage and rearrangement reactions where SpiH3 is responsible for the cleavage of C12a-C12b bond of early typical tetracyclic intermediate to form the oxaspiro structure of 1 and SpiH1, a new member of Baeyer-Villiger monooxygenases catalyzes the crucial cleavage of C12-C12a bond in 1 to give the ring-A opened product of 2. Our work reveals an unprecedented pattern of post-PKS modification on angucycline skeletons that contribute structural diversity and complexity to aromatic polyketides.

Introduction

Angucyclines and angucyclinones are a large family of polycyclic aromatic polyketides mainly produced by actinomycetes. Typical angucyclines possess an unsymmetrically assembled benz[a]anthracene skeleton that biosynthesized by type II polyketide synthases (PKSs) systems.[1–2] This family of compounds exhibit a broad range of biological activities, including anticancer and antibacterial effects, and receive extensive attention from pharmaceutical and biochemical research communities as an important source of lead structures for drug development.[1–3]

The building up of angucycline skeletons in actinomycetes is initiated by the iterative action of a set of minimal PKS enzymes consisting of a β-ketoacyl synthase (KSα), chain length factor (CLF) and an acyl carrier protein (ACP) which catalyze the generation of a highly active poly-β-ketone backbone from acetate, propionate, and malonate precursors. After being processed by the tailoring work flow consisting of a ketoreductase (KR), cyclase (CYC), and aromatase (ARO), the active poly-β-ketone can be transformed into a pool of linear or angular polyketide intermediates such as UMW6 and dehydrorabelomycin (DHR).[1–3] Particularly and importantly, further post-PKS modifications by diverse redox enzymes may take place on these early polyketide backbones and lead to the advanced and highly oxidized products.[4–6]

Among those post-PKS redox modifying enzymes, flavin-dependent monooxygenases (FMOs) have been demonstrated important contributors that introduce structural alterations such as oxidative C-C bond cleavage and carbon rearrangement, therefore, resulting in fascinating atypical angucycline structures.[7–8] For example, UrdM, a bifunctional enzyme with both a reductase domain and an oxygenase domain was proposed to be responsible for the Baeyer-Villiger (BV) oxidative cleavage of ring-A on UWM6, leading to the production of urdamycin L, with a seven-membered lactone structure formed at A-ring[9–10]; and AlpJ, GilOII and JadG, are three Baeyer-Villiger monooxygenases (BVMOs) able to catalyze the crucial C – C

bond cleavage reaction of DHR and cause the ring-B contraction or expansion, resulting in the production of diversified kinamycin[11–12], gilvocarcin[13,15] and jadomycin[14–15] structures.

During our recent work on natural product discovery directed by genome-mining, a type II PKS biosynthetic gene cluster (BGC) was captured from a marine derived actinomycete strain *Streptomyces* sp. HDN155000 due to the presence of a unique set of FMOs which indicated the potential to synthesize diversified angucycline structures.[16] Heterologous expression of the *spi1* cluster led us to isolate and characterize a series of cytotoxic angucycline derivatives including spirocyclione A (**1**), with a novel oxaspiro[benzochromene-2,1'-cyclohexane] architecture, and spirocyclione B (**2**), with an intriguing di-carboxylic substituted benzochromene scaffold. Biosynthesis studies confirmed the unique structures of **1** and **2** were produced from unprecedented flavin-dependent oxidation steps where SpiH3 catalyzed the oxidative cleavage of the C12-C12a bond of an early angular intermediate to form the oxaspiro structure in **1**, and SpiH1, a new member of BVMOs in the antibiotic biosynthesis monooxygenase (ABM) superfamily, was responsible for the C12a-C12b bond cleavage of **1** to give the A-ring opened product of **2**. Here we will report the direct cloning and heterologous expression of the type II PKS *spi1* BGC, the elucidation of new angucycline structures and the enzymatic C – C bond cleavages and rearrangements leading to compounds **1**–**2**.

Results

Identification of Angucycline Biosynthetic Gene Cluster spi1 **in HDN155000.**

Genome mining on the marine derived actinomyces strain *Streptomyces* sp. HDN155000 assisted by online tools of antiSMASH[17] and 2ndfind identified a type II BGC named *spi1* (GenBank accession no. OP009365) which contains a unique set of FMO genes (*spi*H1, *spi*H2 and *spi*H3) with *spi*H1 showing only 46% identity to its nearest homologue of BexI, a proposed monooxygenase in the anthrone biosynthetic pathway (Fig. 1a, **Supplementary Table 5**).[18–19] Cluster alignment revealed the *spi1* BGC spans on a 29 kb of continuous DNA region and contains 26 open reading frames (ORFs, Fig. 1a, **Supplementary Table 5**) with putative genes that encode seven minimal type II polyketide synthase enzymes (*spi*ABCDEFG), ten sugar biosynthesis related enzymes (*spi*LNPQRSTUVW), one drug resistance transporter (*spi*O), and five tailoring enzymes including three monooxygenases (*spi*H1, *spi*H2 and *spi*H3) plus two putative methyltransferases (*spi*M and *spi*I). Apart from the above designated genes, two putative primary metabolic-related genes (*spi*J and *spi*K) and one gene with unpredictable function (*orf1*) were also presented in *spi1*.[20] Detailed protein phylogenetic analysis showed SpiH1 is evolutionarily close to ABM superfamily FMOs but clearly locates in a clade separated from AlpJ/JadG/GilOII/ChaZ/GrhO5, the post-PKS redox enzymes responsible for the biosynthesis of kinamycins (alp)[11], jadomycin (jad)[14–15], gilvocarcin (Gil)[13], chartreusin (Cha)[6], and griseorhodin (grh)[21] (Fig. 1b **and Supplementary Fig. 8**), which indicated the metabolic capacity of *spi*H1 in diversifying angucycline structures. The *spi1* BGC was therefore selected for direct cloning and heterologous expression in *Streptomyces* hosts.

Direct Cloning and Heterologous Expression of spi1 BGC

The *spi1* BGC was cloned into the p15A vector in *Escherichia coli* using Red/ET recombineering technology via the linear plus linear homologous recombination strategy (LLHR)[22–23] to generate the recombinant plasmid p15A1 (Fig. 2a **and Supplementary Fig. 9**). To facilitate site-specific integration and heterologous expression, p15A1 was modified by inserting the *oriT-attP-phiC31* cassette PCR amplified from pR6K-oriT-phiC31[22–23] using the Red/ET linear plus circular homologous recombination method (LCHR), thus yielding the plasmid p15A2 (Fig. 2a, **Supplementary Table 6 and Fig. 9**). Plasmid p15A2 was then introduced into *S. coelicolor* A3(2) to generate strain *S. coelicolor* A3(2)/p15A2. The strain harboring the whole *spi1* BGC was cultured in M1 medium using a shake flask under 30 °C, 200 rpm. However, compared with the background of wild type *S. coelicolor* A3(2), no new peak was detected from the crude extract of *S. coelicolor* A3(2)/p15A2 as analyzed by HPLC (Fig. 2b, **trace ii**). To activate the expression of the *spi1* BGC, one strong promoter, *kasOp**[24], was then inserted downstream to spiH3 to form p15A3 (**Supplementary Fig. 10**). The plasmid p15A3 was retransformed into *S. coelicolor* A3(2) and the resulting strain *S. coelicolor* A3(2)/p15A3 (**Supplementary Fig. 10c**) successfully produced a series of new peaks detected by HPLC at a UV absorption of 210 nm (Fig. 2b, **trace iii**).

Scaled culture (60 L) of *S. coelicolor* A3(2)/p15A3 followed by purification with column chromatography of silica gel, ODS, sephadex LH-20, and semi-HPLC led to the identification of four new angucycline structures named spirocycliones A-B (**1**–**2**) and angumycinones E-F (**3**–**4**) along with two known compounds rabelomycin (**5**)[25] and DHR (**6**)[25] from the crude extract (Figs. 2b-c). The planar structures of compounds **1**–**4** were elucidated based on 1D and 2D NMR data (Fig. 2c **and Supplementary Tables 2–3**). The relative configurations were assigned based on NOESY signals and the calculated i*J*/d*J*-DP4 probability. By applying the ECD calculation method using the time dependent density functional theory (TDDFT) at the B3LYP/6–31 + G(d) level, the absolute configurations of **1**–**2** were defined as (8a*S*, 13*R*)-**1** and 8a*S*-**2**, respectively (**Supplementary Table 1 and** Figs. 1–3). Single-crystal X-ray diffraction analysis by Cu Kα radiation confirmed the absolute configuration of **3** (6a*S*, 7*S*, 8a*R*, 12a*R*, 12b*R*) (Fig. 4, CCDC 2181459). Considering the same biosynthetic origin, the absolute configuration of **4** was presumed to be consistent with **3**. Hence, the absolute configuration of **4** was determined as 6a*S*, 8a*R*, 12a*R*, 12b*R*.

Among those structures, compound **1** represents the first example of angucycline derivatives with an oxaspiro[benzochromene-2,1'-cyclohexane] architecture, and compound **2** possesses an intriguing benzochromene scaffold appended with two carboxylic acid terminals which probably derived from the A ring cleavage of compound **1**. These obtained structures exhibited cytotoxicity against a panel of cancer cell lines with compound **4** showing promissing activity to the multidrug-resistant human small-cell lung carcinoma cell line of H69AR with an IC_{50} value of 0.97 μM, which was comparable to the positive control of adriamycin (ADM, Table 1).

Table 1
In Vitro Antitumor Activities of the spirocycliones (IC_{50}, μM).

Compd	MDA-MB-231	K562	ASPC-1	H69AR	H69
1	12.65	> 50	> 50	> 50	> 50
2	> 50	> 50	> 50	23.39	> 50
3	25	4.38	> 50	25	> 25
4	2.16	2.05	8.23	0.97	10.48
ADM	0.31	0.24	0.22	0.52	0.36

FMOs of SpiH1, SpiH2 and SpiH3 Involved in the Biosynthesis of Atypical Angucyclines

The structural novelty and bioactivity presented by these angucyclines increased our interest in studying their biosynthetic routes, especially the formation of the oxaspiro structure in rings A and B of **1** and the cleavage of ring A in **2**. Initially, to reconfirm the correlation of the *spi1*-cluster with the production of these angucyclines, *spi*A, the key gene which encodes the type II polyketide synthase was inactivated from the *spi1* BGC using LCHR in *E. coli* GB08-red and the mutant plasmid was re-transformed into *S. coelicolor* A3(2); as a result, the production of new peaks were abolished **(Supplementary Fig. 11a**). To rule out the heterologous host redox modification effects on the formation of novel structures 1–2, the p15A3 plasmid was transformed into different host strains of *S. venezuelae* (ISP 5230) and *S. lividans* K4-114, and the productions of **1** and **2** were detected from both cultures (**Supplementary Fig. 11b**), reconfirming the involvement of *spi1* BGC in the biosynthesis of the above atypical angucycline structures.

It has been reported that the biosynthesis of angucycline structures share an initial biosynthetic pathway, which includes the formation of the polyketide backbone and early processing steps on it to provide the common intermediates such as UWM6[1]. The highly active intermediate UWM6 could undergo complex oxidative modifications and carbon skeleton rearrangements to give diversified tetracyclic or tricyclic frameworks. During this process, redox tailoring enzymes, especially the FMOs, are revealed to play the pivotal roles in modifying the early angular intermediates and generating structural complexity and diversity (Fig. 3).

To gain a better understanding of the interesting rearrangement cascade from the early tetracyclic intermediate into to the final products including **1**–**2**, we focused on the three FMOs of SpiH1, SpiH2 and SpiH3, which were thought to be responsible for the post-PKS modification of early angular skeletons. At first, we inactivated spiH1, spiH2, and spiH3 individually from p15A3 using the Red/ET LCHR method to give p15A3KOH1, p15A3KOH2 and p15A3KOH3, which were then transformed and expressed in *S. coelicolor* A3(2) (**Supplementary Fig. 12**).

As a result, the mutant plasmid p15A3KOH1 failed to produce compound **2** while maintaining the ability to produce compound **1**, however, the production of **1**–**2** were both abolished within the p15A3KOH2 and p15A3KOH3 mutants (Fig. 2a, **trace v-vii**). Chemical analysis of the *S. coelicolor* A3(2)/p15A3KOH1 strain led us to isolate a new tetracyclic angular structure gephyromycin E (**8**) together with a known compound gephyromycin (**7**), which have been reported as products from early oxidative modification steps[26] catalyzed by SpiH2 and SpiH3 homologues (Fig. 2a, **trace v and Supplementary Figs. 5–6**). And two extra known compounds rabelomycin (**5**) together with RM20C (**9**), whose skeleton was reported to be generated from the spontaneous cyclization of the linear decaketide skeleton[27] were accumulated and obtained from the strains of *S. coelicolor* A3(2)/p15A3KOH2 and *S. coelicolor* A3(2)/p15A3KOH3, respectively (Fig. 2a, **trace vi and trace vii**). Those results indicated that SpiH2 and SpiH3 probably worked upstream in the biosynthetic process relative to SpiH1 and converted early angular intermediates such as UWM6 into oxidized structures, including the oxaspiro product **1** and other oxidative modified structures such as **3**–**8**, while SpiH1 worked downstream to convert **1** into the ring-opened structure of **2** (Fig. 3).

SpiH2 and SpiH3 Are Responsible for the Formation of Spirocyclione A (1)

Phylogenetic analysis showed SpiH2 clustered with PgaM[28], BexM[19] and UrdM[9], which are two-domain flavoproteins that contain an N-terminal domain homologous to FAD-dependent monooxygenases fused to a C-terminal domain homologous to SDRs via a short linker region (**Supplementary Figs. 13–14**). To test the *in vitro* function of SpiH2 in the formation of compound **1**, we tried to purify SpiH2 expressed in *E. coli* BL21(DE3), however, as in similar cases reported for its homologues, the protein was mostly produced as inclusion bodies[29], which prevented the *in vitro* attempts. We then tested the *in vivo* activity of SpiH2 within an alternative host. Plasmid p15A5 was constructed by inserting spiH2 into the p15A backbone (**Supplementary Fig. 15b**) and transformed into *S. coelicolor* A3(2). The resulting strain *S. coelicolor* A3(2)/p15A5 was fed with extracts from *S. coelicolor* A3(2)/p15A3KOH2 (extract-1) and BAP1/pGro7/pXY-1/pXY-3/pXY-6 (extract-2)[30], both of which have the capability to supply early angular intermediates such as UWM6 and SF2315A[31], which are presumed precursors of **1**.

The cultures were then subjected to LC-MS detection, but compound **1** was not detected from the fermentation products (Fig. 4a), which revealed SpiH2 was not capable of converting early angular intermediates to compound **1**. However, interestingly one new peak, characterized as 7-hydroxyfridamycin E (**10**)[32] was identified in the mixture (Fig. 4A). To further test the activity of SpiH2 in correlation with the production of **10**, we fed rabelomycin (**5**), a proposed precursor of **10** to *S. coelicolor* A3(2)/p15A5. The resulting HPLC profile indicated one extra peak, which was further identified as urdamycin L (**12**), the proposed BV oxidation product of **10** catalyzed by the SpiH2 homologue UrdM[9–10], which experimentally confirmed the BV oxidative C-C bond cleavage ability of SpiH2 on an agucycline skeleton.

To continue interrogating the biosynthesis of **1**, we focused on SpiH3, which was also predicted to be an NADPH-dependent flavoprotein hydroxylase based on phylogenetic analysis and clustered with PgaE[28],

BexE[19], and UrdE[9] (**Supplementary Fig. 13**). The gene spiH3 was inserted into the pColdI backbone to construct plasmid pColdIH3. An induced culture of BL21(DE3) containing pColdIH3 fed with extract 2 successfully produced **1** (Fig. 4b), which preliminarily confirmed SpiH3 was able to convert early angular intermediates to the oxaspiro[5.5]undecane featured compound **1**. We then planned to test the function of SpiH3 *in vitro* using UWM6 and SF2315A as substrates, the most possible precursors leading to **1**. However, efforts were obstructed by failing in preparation of both UWM6 and SF2315A due to their highly active and unstable properties. Instead, an analogue of SF2315A, characterized as a new compound named kanglemycin D (**11**) was obtained from the *S. coelicolor* A3(2)/p15A3KOH1 culture. We then purified N-His_6-tagged SpiH3 from *E. coli* BL21(DE3)/pColdIH3 (**Supplementary Fig. 18a**) and tested its enzymatic activity with compound **11** as a substrate instead of UWM6 and SF2315A. As a result, a new peak was detected from the reaction mixture. Due to the low catalytic efficacy and resulting trace amount of output, we failed to purify it. However, the MS spectrum showed an ion peak at m/z 356.89 $[M + H]^+$, which suggested SpiH3 was able to introduce an oxygen atom into the skeleton of **11** (**Supplementary Fig. 18b**), supporting the hypothesis that SpiH3 could catalyze oxidation of early angular intermediates to give compound **1**.

Based on the above results, we illustrated the conversion steps from early angular intermediates to the novel oxaspiro architecture of **1**, which involved SpiH2 and SpiH3 working cooperatively for sequential oxidations. UWM6, the early common intermediate, was transformed into SF2315A probably catalyzed by SpiH2 and SpiH3 through successive redox reactions. The Δ12b double bond of SF2315A was then opened by SpiH3 through another flavin-dependent oxidation step to give the proposed intermediate **1'**, which further underwent C12a-C12b carbon bond cleavage and ring rearrangement to generate the final product of **1** (Fig. 4c). SpiH3 homologues have been well investigated for their capabilities of hydroxylating early angular intermediates at the C1 position[9,25], while the production of compound **1** represents the first example of a flavin-dependent C12a-C12b carbon bond cleavage and hydroxylation at the C12a position, thus resulting in the formation of the oxaspiro[5.5]undecane structure in rings A and B.

To consolidate the proposed pathway from SF2315A to **1** and better understand the flavin-dependent SpiH3 catalyzed ring rearrangement process, we conducted density functional theory (DFT) calculations on the reaction between SF2315A and the simplified coenzyme factor Fl-OO^-. As shown in Fig. 5, the processes started with the 1,4-michael addition of Fl-OO^- to the naphthoquinone part of SF 2315A to easily form the conjugate **1'** via transition state TS1 (21.0 kcal mol-1), then tautomerized into enol form **1'a**. The TS2 is calculated as high as 31.3 kcal mol^{-1}, indicating that the epoxidation of the enol double bond cannot smoothly occur at room temperature without the catalysis of SpiH3. Once the departure of Fl-O^-, the process is hugely exothermic and to obtain the epoxy compound **1'b**, which could hardly go through the bond cleavage reaction with the energy barrier TS3' is 64.1 kcal mol^{-1} (**Supplementary Fig. 16**). However, with the aid of imidazole and its conjugated acid, which built up proton shuttles, the latter processes could undergo rapidly at room temperature. This provided the other evidence that the enzyme SpiH3 participates in the whole processes of rearrangement. The epoxy ring expanded into the seven-membered compound **1"** through a bond cleavage reaction, then the intramolecular attack of the

hydroxyl group to give the bridged-ring **1'''**. Finally, through sequential reactions including the ether bond break and the capture of proton to afford the spiral compound **1**.

SpiH1 Is the Key Enzyme for the Biosynthesis of Spirocyclione B (2)

Phylogenetic analysis identified SpiH1 as an BVMO within the ABM superfamily, but clustered in a different clade from other characterized BVMOs in type II PKS biosynthesis like, for example, JadG and AlpJ, the key enzymes responsible for ring B cleavage of benz[a]anthracene backbones (Fig. 1b). To reconfirm SpiH1 was directly related to the formation of **2**, *in trans* complementation of the SpiH1 deficiency was achieved by transforming *S. coelicolor* A3(2) with p15A6, a plasmid with insertion of spiH1 into p15A3KOH1 backbone (Fig. 2b, **trace viii, Supplementary Fig. 17**). Results showed the production of **2** was successfully recovered in the *S. coelicolor* A3(2)/p15A6 strain, verifying the involvement of SpiH1 in **2** formation. Next, compound **1**, the postulated intermediate leading to **2** was added to the culture of the spiH1 over-expressed strain, which was achieved by transforming *S. coelicolor* A3(2) with p15A4, a plasmid carrying only spiH1within the p15A backbone (**Supplementary Fig. 15a**). As shown in Fig. 6a, LC-MS analysis revealed **2** was successfully produced in the culture, which further confirmed the function of SpiH1 in converting **1** to **2**. To further investigate the BV oxidation activity of SpiH1, N-His_6-tagged SpiH1 was purified from *E. coli* BL21(DE3)/pET28a-H1 to near homogeneity (**Supplementary Fig. 20a**). Experiments were processed *in vitro* by incubating **1** with SpiH1, FAD, NADPH and *E. coli* flavin reductase (Fre), which is known to regenerate $FADH_2$ from FAD using NADPH[11]. As shown in Fig. 6b, the production of **2** in the reaction mixture was detected by HPLC trace. To further test the substrate promiscuity of SpiH1, compounds **3**–**5**, whose structures containing C12 carbonyl groups were incubated *in vitro* with SpiH1, but no obvious changes for all the tested compounds were observed (data not shown), showing the relatively low promiscuity for SpiH1.

Based on above results, the conversion steps from the oxaspiro structure of **1** to the ring A-opened product of **2** was proposed: BV reaction on **1** catalyzed by SpiH1 introduced an oxygen atom adjacent to the active 12-carbonyl group, thus generating the ester intermediate **2'**, which subsequently underwent a spontaneous rearrangement reaction and oxidation steps to give the final ring A opened product of **2** (Fig. 6a)

Docking and Mutagenesis Studies Revealing Key Residues for the Function of SpiH1

Sequence alignment of SpiH1 with AlpJ and other BVMOs in the ABM superfamily revealed the conserved residues in N-terminal (GxSxxxG) and C-terminal (YxQW), which was consistent with the BV oxidation activity of SpiH1 (**Supplementary Fig. 19**). To further understand the role of SpiH1 during the intriguing transformation from **1** to **2**, we then performed AlphaFold2 assisted protein analysis on SpiH1[33]. The overall structure of SpiH1 consists of six α helices and nine antiparallel β sheets, which make two hydrophobic pockets within the C-terminal pocket in the “open” conformation accessible to substrate while the N-terminal is buried and not easy for reactants to enter (**Supplementary Figs. 20b-c**). In addition, both pockets showed no FAD-like cofactors binding sites, which is the typical characteristic for FMOs in

the ABM superfamily.[1] Above features highly resembled to the three-dimensional conformation of the well characterized AlpJ. Detailed analysis of the sequence also provided the conserved residues of His54 and Trp68 in the N-terminal, and Tyr170, Gln172 and Trp173 in the C-terminal. SpiH1 and compound **1** were then subjected to docking analysis using AutoDock Vina[34]. The best binding conformations revealed most conserved residues are positioned toward the catalytic cavity, except for Tyr170, which was reported to be the key residue for stabilization of domain interface, being stretched outside. Importantly, the size of the SpiH1 active site was predicted to be much bigger than that of any previously reported AlpJ family of oxygenases with five proposed catalytic residues of Arg125, Asn169, Tyr179, Tyr182 and Asn188 folded into the cavity, which suggested a different mechanism of substrate binding or catalysis for SpiH1 (Figs. 6d-e).

On the basis of the above information, the conserved sites including residues at the intramolecular domain interface (His54 and Tyr170) and residues reported responsible for substrate binding (Val64, Trp68, Trp173), together with residues specifically presented in the SpiH1 catalytic pocket (Arg125, Asn169, Tyr179, Tyr182 and Asn188) and a conservative site of Gln172 in the C-terminal were mutated to alanine. The activities of SpiH1 and its mutants were evaluated by monitoring the consumption of the substrate **1**, and the reaction mixture with boiled SpiH1 was used as a negative control.

As shown in Fig. 6c, the activities of H54A, W68A, R125A, Y170A, W173A, Y182A and N188A were drastically decreased by more than 70% compared with wild-type SpiH1. For other mutants like N169A, Q172A, and Y179A, activity was only slightly affected. The above results support both the N- and C-terminal putative active sites as being vital for the activity of SpiH1, with the C-terminal “open” to the reactants and the N-terminal helping to stabilize the active conformation, where Arg125 and Asn188 together with Tyr182 form strong hydrogen bonds with the C1 carbonyl and C13 hydroxyl groups of **1**, thus exposing the C12 carbonyl to the cofactor of peroxyflavin and facilitating the nucleophilic attack initiated BV oxidation. Compared with AlpJ, the bigger active sites of SpiH1 may allow the accommodation of substrate **1**, which needs more space than DHR, the nearly planar structured substrate of AlpJ.

In conclusion, heterologous expression and mutational biosynthetic studies of a type II PKS BGC led us to characterize six new angucycline variant structures (**1**–**4**, **8**, **11**). Interestingly, compound **1** represents the first example of angucycline derivatives with an oxaspiro[5.5]undecane ring system and compound **2** possesses a benzochromene scaffold bearing two carboxylic acid substitutions derived from the oxidative cleavage of compound **1** in ring-A. Meanwhile, compound **1** exhibited promising cytotoxicity against triple-negative breast cancer (TNBC) cell line of MDA-MB-231, and compound **2** showed cytotoxicity to multidrug-resistant human small-cell lung carcinoma cell line of H69AR. Biosynthesis studies based on *in vivo* biotransformation experiments revealed the formation of **1** resulted from sequential flavin dependent oxidative reactions on the structure of the early tetracyclic angular intermediates such as UWM6 catalyzed by two FMOs of SpiH2 and SpiH3, while SpiH1, identified as a new member of ABM super family FMOs, was unambiguously confirmed to catalyze the transformation from **1** to **2** via BV oxidation adjacent to the C12 carbonyl followed by hydrolysis steps, which represented

the first example of BV oxidative cleavage of ring A on oxaspiro angucycline derivatives. AlphaFold assisted analysis and site-directed mutagenesis experiments revealed the structure of SpiH1 was conformationally similar to the AlpJ family of oxygenases but possessed a more relaxed space in the catalytic cavity with a triad of Arg125, Tyr182 and Asn188 presented as active sites, which may facilitate the loading of the more stereoscopic stretched substrate of **1** and the peroxyflavin dependent nucleophilic attack at the of C12 carbonyl position. The elucidation of new compounds in this study enriches the structural diversity of angucycline-like chemical entities and the discovery of the new function of the above enzymes expands the catalytic repertoire of naturally occurring flavoproteins in aromatic polyketide biosynthesis, and enlightens ongoing chemical engineering and molecular design work based on FMOs catalyzed oxidative reaction cascades.

Methods

General Experimental Procedures

Optical rotations were obtained on a JASCO-1020 digital polarimeter (JASCO, Tokyo, Japan) using MeOH as the solvent at 25 ℃. IR spectra were recorded on a Nicolet NEXUS 470 spectrophotometer (Thermo Scientific, Beijing, China) in KBr disks. UV data were measured on a Beckman DU 640 spectrophotometer (Beckman Ltd., Shanghai, China). HRESIMS spectra were measured on a Micromass EI-4000 (Autospec-Ultima-TOF, Waters, Shanghai, China). NMR spectra was performed on BRUKER AVANCE NEO 400 MHz (Bruker, Beijing, China) and Agilent 500 MHz DD_2 (Agilent, Beijing, China) and JEOL JNM-ECP600 spectrometers (JEOL, Beijing, China), and the 1D and 2D spectra were referenced to the residual deuterated solvent peaks. Conformational searches were run, employing Spartan'14, based on the MMFF (Merck Molecular Force Field). All conformers were further optimized with DFT calculations at the B3LYP/6–31 + G(d) level by using the Gaussian 09 program. The ECD spectra were measured on a JASCO J-715 spectropolarimeter. X-ray crystal data were measured on an Agilent Gemini Ultra diffractometer with Cu Kα radiation. The silica gel (100–200 and 200–300 mesh, Qingdao Marine Chemical Factory, Qingdao, China), reversed-phase silica gel (50 μm; Silicycle, Shanghai, China), and Sephadex LH-20 gel (GE Healthcare, Bio-Sciences Corp, Piscataway, NJ, USA) were used for column chromatography (CC). An ODS column (YMC-Pack ODS-A, 10 × 250 mm, 5 μm, 3 mL/min, YMC Co., Ltd.) was used for semi-preparative HPLC. The structure of proteins was predicted through AlphaFold2[33]. All structural figures were prepared using PyMol (The PyMol Molecular Graphics System, Version 2.3, Schrödinger, LLC).

Microorganisms, plasmids and reagents

Streptomyces sp. HDN155000 (GenBank No. OP001709) was isolated from a sediment sample collected from the South China Sea (125°28.550' E, 29°1.618' N). The strain was deposited at the Key Laboratory of Marine Drugs, the Ministry of Education of China, School of Medicine and Pharmacy, Ocean University of China, Qingdao, People's Republic of China. Primers and plasmid sequencing were provided by the

Shanghai Sangon Biotech Co., Ltd (**Supplementary Table 6**).The strains, mutants and plasmids used in this study are listed in **Supplementary Table 7**.

DNA isolation, sequencing and bioinformatics analysis

The seed liquor of *Streptomyces* sp. HDN155000 was cultivated in 250 mL Erlenmeyer flasks containing 50 mL of culture medium composed of 0.5% peptone, 0.1% yeast extract, 0.1% glucose, 0.01% iron phosphate, pH = 7.0 (in seawater collected from Huiquan Bay, Yellow Sea) and cultured at 30°C for 2–3 days on a rotary shaker at 200 rpm. Genomic DNA extraction was carried out as described previously.[22] Whole genome sequencing was completed by Novogene Biotechnology (China) using a PacBio Sequel platform (https://en.novogene.com/technology/platforms/). The biosynthetic gene clusters in the genome were analyzed by antiSMASH (https://antismash.secondarymetabolites.org/#!/start)[17] and 2ndfind (https://biosyn.nih.go.jp/2ndfind/). The sequence of the *spi1* cluster was submitted to the GenBank database (OP009365).**Supplementary Table 5** shows the gene annotation of the identified angucycline biosynthetic gene cluster (*spi1*), which is depicted in **Supplementary Fig. 8**.

Direct cloning of spi1 gene cluster and construction of expression vector

The 29-kb *spi1* gene cluster was transferred to *S. coelicolor* A3(2) using direct cloning by means of ExoCET.[23] The prepared genomic DNA (50 μg) above was digested with NdeI-NaeI, extracted with phenol–chloroform–isoamyl alcohol (25:24:1, pH 8.0) and precipitated with ethanol. The DNA was dissolved in ddH_2O. The vector p15A carrying homology arms of *spi1* genes was amplified with PCR using the primeSTAR Max DNA Polymerase (Takara). The digested genomic DNA (10 μg) and amplified p15A (200 ng) were assembled *in vitro* and then electroporated into the *E. coli* harboring the plasmid pSC101-BAD-ETgA for homologous recombination.[35] The recombinant plasmid p15A1 containing the *spi* fragment was identified with KpnI restriction analysis and further verified by restriction enzymes after re-transformation. Thereafter it was modified via LCHR (linear plus circular homologous recombination) by Red recombineering[35] to insert the *oriT-attP-phiC31* cassette from pR6K-oriT-phiC31 amplified with PCR to form p15A2 for targeting and integration into the heterologous host genome.

Promoter engineering

The promoter cassette, *hyg-kasOp**, which was PCR amplified using p15A-cm-57p-hyg-kasOp [24,36] as a template, was inserted into the p15A vector (digested with PacI) to afford p15A-cm-hyg-*kasOp**. The *hyg-kasOp** cassette amplified from p15A-cm-57p-hyg-kasOp* with appropriate primers and flanked with 40 bp homology arms was inserted downstream of *spi*H3 in p15A2 by LCHR to obtain p15A3.

Heterologous expression, fermentation, and isolation of compounds in S. coelicolor A3(2)

The plasmids p15A2 and p15A3 were transformed into *S. coelicolor* A3(2) to give the strains *S. coelicolor* A3(2)/p15A2 and *S. coelicolor* A3(2)/p15A3 via conjugation from *E. coli* ET12567/pUZ8002 according to methods described in prior literature.[37] The trans-conjugants for each plasmid were inoculated into 100 mL M1 fermentation medium (soluble starch 1%, yeast extract 0.4%, tryptone 0.2%) in 500 mL Erlenmeyer

flasks and incubated at 30°C for 8 days (**Supplementary Fig. 10**). Metabolites were extracted using EtOAc (3×60 L) to generate extract (12.5 g). The extract from *S. coelicolor* A3(2)/p15A3 was applied to a C_{18} column using a stepped gradient elution of MeOH-H_2O, yielding seven subfractions (Fr.1 – Fr.7, 1–100%). Fr.5 was separated by an LH-20 column to obtain four subfractions (Fr.5.1 – Fr.5.4). Fr.5.3 was purified by semipreparative HPLC (46:54 MeOH-H2O, 3 mL/min) to afford **1** (15 mg, t_R= 35.3 min) and **2** (4.6 mg, t_R= 36.1 min). Fr.5.1 was separated by semipreparative HPLC (40:60 MeOH-H_2O, 3 mL/min) to obtain **3** (7 mg, t_R= 26.3 min). Fr.5.2 was separated by semipreparative HPLC (58:42 MeOH-H_2O, 3 mL/min) to obtain **4** (25 mg, t_R = 30.9 min). Fr.5.4 and Fr.7 were also separated by semipreparative HPLC (60:40; 80:20 MeOH-H_2O, 3 mL/min, respectively) to obtain **5** (50 mg, t_R = 27.7 min) and **6** (45 mg, t_R = 47.5 min).

In-frame deletion procedure

The target sequences (*spi*A, *spi*H1, *spi*H2, *spi*H3) were replaced by the *cm-ccdB* cassette amplified from the p15A-cm-ccdB backbone containing PacI sites at both ends using LCHR in GBred-gyrA462[38]. The recombinant plasmids carrying the *cm-ccdB* were identified by restriction enzyme analysis of colonies selected on LB plates supplemented with chloramphenicol (cm). Thereafter, the correct plasmids were digested with PacI to release the *cm-ccdB* cassette, self-ligated with T_4 DNA ligase and electroporated into *E. coli* GB2005 cells. The plasmids without the cassette *cm-ccdB* were excluded by restriction enzyme analysis of colonies selected on LB plates supplemented with apramycin (Apra), and then the plasmids p15A3/KOA, p15A3/KOH1, p15A3/KOH2, p15A3/KOH3 were obtained.

Complementation of gene spi**H1**

In order to verify the function of *spi*H1, the *spi*H1 gene was *in trans* complemented by adding *spi*H1 into the plasmid p15A3/KOH1. The *amp-ccdb* cassette containing PmeI sites at both ends was inserted into downstream of *spi*H3 in p15A3/KOH1 via LCHR (**Supplementary Fig. 16**). The recombinant plasmid was linearized by PmeI digestion and re-transformed in GB2005. The correct plasmids identified by restriction digestion were confirmed by sequencing. The primers involved above are listed in **Supplementary Table 6**.

Isolation and structure elucidation of p15A3 mutant strain

A total of 28 L, 5 L, 25 L cultures of p15A3/KOH1 (6.8 g), p15A3/KOH2 (1.5 g), p15A3/KOH3 (10.0 g) in M1 medium were prepared for compound isolation. This extracts was subjected to C_{18} column chromatography using a stepped gradient elution of MeOH-H_2O, yielding subfractions for further isolation. Fr.3 in p15A3/KOH1 (40:60, MeOH:H_2O) was separated by semipreparative HPLC (38:62, MeCN-H_2O, 3 mL/min) to afford the accumulated compounds **7** (1 g, t_R = 28.2 min) and **8** (100 mg, t_R = 32.4 min). Fr.4 in p15A3/KOH2 (60:40, MeOH:H_2O) was separated by semipreparative HPLC (54:46, MeOH-H_2O, 3 mL/min) to afford the accumulated compound **5** (10 mg, t_R = 27.7 min). Fr.3 in p15A3/KOH3 (60:40, MeOH:H_2O) was separated by semipreparative HPLC (25:75, MeCN-H_2O, 3 mL/min) to afford the accumulated compound **9** (6 mg, t_R = 33.5 min).

Cloning, expression, feeding and characterization of enzymes

Sequential cloning

Primers used for amplification of the plasmids from the genomic DNA of *Streptomyces* sp. HDN155000 and the plasmid pET28a-H1 are listed in **Supplementary Table 6**. The resulting DNA fragments were cloned into the commercial pET28a vector or pColdI vector via ligation cloning and the ligation mixture was transformed into *E. coli* DH5α. The resulting constructs were verified by restriction digest and DNA sequencing. The correct plasmids were transformed into *E. coli* BL21(DE3) for heterologous expression of the His-tagged protein.

Protein expression and purification

DNA fragments containing target genes including *spi*H1, *spi*H2 and *spi*H3 were amplified from genomic DNA of HDN155000 with primers listed in **Supplementary Table 6**. The purified PCR products were ligated with linearized pColdI or pET28a (linearized by NdeI, HindIII) to afford pET28a-H1, pET28a-H2, pColdH3. The plasmids were separately introduced into *E. coli* BL21(DE3). The transformants were cultivated in 1 L LB medium at 37°C (220 rpm) until the OD_{600} value reached 0.4–0.6. The cultures were cooled to 4°C and induced with 0.1–0.2 mM IPTG and continued to cultivate at 16°C (220 rpm) for 18 hours. After centrifugation at 8000 rpm for 10 min, cells were resuspended in 25 mL lysis buffer (50 mM Tris-Hcl, 500 mM NaCl, 10% glycerol, pH 7.5) and lysed on ice by sonication. After centrifugation at 12000 rpm for 30 min, the supernatant was filtered and purified using a Histrap column. The proteins were pooled and desalted by a PD10 column (GE Healthcare) with 50 mM Tris-Hcl, 50 mM NaCl (pH 7.5) and 5% glycerol and stored at -80°C.

In vitro assay

The pET28a-H1 catalyzed reaction was carried out in a 100 μL reaction containing 50 mM Tris-HCl buffer (pH 7.5), 100 μM substrate, 1 mM NADPH, 20 μM FAD, 10 μM Fre, 10 μM pET28a-H1. After incubation at 30° C for 1 hour, 100 μL acetonitrile was added to quench the reaction. Then, the reaction mixture was centrifuged at 14000 rpm for 10 min, and the supernatant was subjected to UPLC-MS analysis. The UPLC-MS analysis was performed with 45 min gradient elution system from 30 to 90% (1–35 min), 100% (35–40 min) and 30% (40–45 min) acetonitrile using a BEH C_{18} column (1.7 μm, 2.1 × 50 mm) in water supplied with 0.1% formic acid at a flow rate of 0.5 mL/min. The pColdH3-catalyzed reaction using extract 2 as the substrate was conducted in the same condition using 1 mM NADPH as a cofactor. After incubation at 30° C for 30 min, the reaction was quenched.

Chemical complementation

The mutants *S. coelicolor* A3(2)/p15A4 and *S. coelicolor* A3(2)/p15A5 were cultured in a 100 mL scale at 30 ℃ in fermentation medium. After 4 days cultivation, extract **1** (1 mg/mL), extract **2** (1 mg/mL) and

compound **5** (100 mM) dissolved in DMSO were individually supplemented into *S. coelicolor* A3(2)/p15A5 fermentation broth and cultured for another 36 hours. The metabolic extract was analyzed by HPLC. The HPLC analysis was performed with a 45 min gradient elution system from 30–90% (3–35 min), 100% (35–40 min) and 30% (40–45 min) acetonitrile using a BEH C_{18} column (1.7 μm, 2.1 × 50 mm) in water supplied with 0.1% formic acid at a flow rate of 0.5 mL/min.

Cytotoxicity assay

Cytotoxic activities of compounds **1–4**, **8**, **11** were evaluated against K562 (using the MTT method), L-02, H69AR, H69, MDA-MB-231, ASPC-1 (using the SRB method) cell lines. ADM was used as a positive control, and the IC_{50} values are shown in Table 1. The detailed methodologies for biological testing have been described in previous reports[39–40].

Computational methods

All the DFT calculations were performed with Gaussian 09[41]. Geometry optimizations of the ground state and transition structures were carried out at the M062X level of theory[42] with the 6-31G(d) basis set in water using the CPCM solvation model[43]. Vibrational frequencies were computed at the same level to verify that optimized structures are local minimums or transition states. Then the energies of the optimized structures in water were computed at the more accurate M062X/6-311 + G(d,p) level with the CPCM model.

Data availability

Data supporting the findings of this work are available within the paper and its Supplementary Information files. A reporting summary for this Article is available as a Supplementary Information file. The spirocyclione BGC has been deposited in Genbank under accession number OP009365 [https://www.ncbi.nlm.nih.gov/nuccore/OP009365]. Source data are provided with this paper.

Declarations

Acknowledgements

We are grateful to Youming Zhang from Shandong University for providing materials for Red/ET cloning, Ming Jiang from Shanghai Jiao Tong University for sharing the *E. coli* strains which produce type II PKS intermediates, Keqiang Fan and Guohui Pan from Institute of Microbiology, Chinese Academy of Sciences for providing Fre proteins. This work was supported by the National Natural Science Foundation of China (41976105, 81991522), NSFC-Shandong Joint Fund (U1906212), Hainan Provincial Joint Project of Sanya Yazhou Bay Science and Technology City (2021CXLH0012), Marine S&T Fund of Shandong Province for Pilot National Laboratory for Marine Science and Technology (Qingdao) (2022QNLM030003-1, 2022QNLM030003-2), Taishan Scholar Youth Expert Program in Shandong Province (tsqn 201812021, tsqn 202103153), Major Basic Research Programs of Natural Science Foundation of Shandong Province (ZR2021ZD28).

Author contributions

D. Li and G. Zhang designed and supervised this study; X.X., C.M, and F.Z. performed gene cloning, point mutations, protein purification, in vivo deletion; G.Z. and X.X. performed bioinformatic analyses, in vitro experiments; X.X., L.Z., and F.Z. fermented and purified compounds and elucidated the structure of compounds; Y.C. processed the DFT calculations; T.Z., Q.C. and B.A.P. read and revised the manuscript; D.L., G.Z. and X.X. wrote and revised the manuscript.

Competing interests

The authors declare no competing interests.

References

1. Kharel, M. K. *et al*. Angucyclines: Biosynthesis, mode-of-action, new natural products, and synthesis.Nat. Prod. Rep. **29**, 264–325 (2012).
2. Mikhaylov, A. A., Ikonnikovab, V. A., and Solyev, P. N. Disclosing biosynthetic connections and functions of atypical angucyclinones with a fragmented C-ring. Nat. Prod. Rep. **38**, 1506–1518 (2021).
3. Cao, M. *et al*. Cryptic sulfur incorporation in thioangucycline biosynthesis. Angew. Chem. Int. Ed. **60**, 26378–26384 (2021).
4. Chen, S.C., Zhang, C., and Zhang, L. Investigation of the molecular landscape of bacterial aromatic polyketides by global analysis of type II polyketide synthases. Angew. Chem. Int. Ed. **61**, 1–9 (2022).
5. Tolmie, C. Smit, M. S. Opperman, D. J. Native roles of Baeyer–Villiger monooxygenases in the microbial metabolism of natural compounds. Nat. Prod. Rep. **36**, 326–353 (2019).
6. Jiao, F. W. *et al*. An NADPH-dependent ketoreductase catalyses the tetracyclic to pentacyclic skeletal rearrangement in chartreusin biosynthesis. Angew. Chem. Int. Ed. **60**, 26378–26384 (2021).
7. Huang, C. S. *et al*. Molecular basis of dimer formation during the biosynthesis of benzofluorene-containing atypical angucyclines. Nat. Commun. **9**, 2088–2097 (2018).
8. Gober, R., Wheelera, R., and Rohr J. Post-PKS enzyme complexes. Med. Chem. Commun. **10**, 1855–1866 (2019).
9. Rix, U., Remsing, L., Hoffmeister, D., Bechthold, A. and Rohr, J. Urdamycin L: a novel metabolic shunt product that provides evidence for the role of the urdM gene in the Urdamycin A biosynthetic pathway of *Streptomyces fradiae* Tü 2717. Chembiochem **4**, 109–111 (2003).
10. Kobylyanskyy, A., Ostash, B., Fedorenko, V. Heterologous cross-expression of oxygenase and glycosyltransferase genes in streptomycetes, producing angucyclic antibiotics. Tsitol Genet. **43**, 55–62 (2009).
11. Pan, G. *et al*. Structure and function of a C – C bond cleaving oxygenase in atypical angucycline biosynthesis. ACS. Chem. Biol. **12**, 142–152 (2017).

12. Wang, B. Kinamycin biosynthesis employs a conserved pair of oxidases for B-ring contraction. Chem. Commun. **51**, 8845–8848 (2015).
13. Pahari, P. Kharel, M.K. Shepherd, M.D., van Lanen, S.G., and Rohr, J. Enzymatic total synthesis of defucogilvocarcin M and its implications for Gilvocarcin biosynthesis. Angew. Chem. Int. Ed. **51**, 1216–1220 (2012).
14. Fan, K. *et al*. Identification of JadG as the B ring opening oxygenase catalyzing the oxidative C-C bond cleavage reaction in Jadomycin biosynthesis.Chem. Biol. **19**, 1381–1390 (2012).
15. Tibrewal, N. *et al*. Baeyer-Villiger C-C bond cleavage reaction in Gilvocarcin and Jadomycin biosynthesis. J. Am. Chem. Soc. **134**, 18181–18184 (2012).
16. Huo, L. J. *et al*. Heterologous expression of bacterial natural product biosynthetic pathways. Nat. Prod. Rep. **36**, 1412–1436 (2019).
17. Blin, K. Medema, M.H., Kottmann, R., Lee, S. Y., and Weber, T. The antiSMASH database, a comprehensive database of microbial secondary metabolite biosynthetic gene clusters. Nucleic. Acids. Res. **45**, D555-D559 (2017).
18. Jackson, D. R. *et al*. Biosynthesis of diverse type II polyketide core structures in *Streptomyces coelicolor* M1152. ACS. Chem. Biol. **11**, 1137–1147 (2016).
19. Sasaki, E., Ogasawara, Y., Liu, H. W. A biosynthetic pathway for BE-7585A, a 2-thiosugar-containing angucycline-type natural product. J. Am. Chem. Soc. **132**, 7405–7417 (2010).
20. Mo, J. *et al*. Cloning and identification of the Frigocyclinone biosynthetic gene cluster from *Streptomyces griseus* strain NTK 97. Biosci. Biotechnol. Biochem. **83**, 2082–2089 (2019).
21. Frensch, B. *et al*. Enzymatic spiroketal formation via oxidative rearrangement of pentangular polyketides. Nat. Commun. **12**, 1431–1443 (2021).
22. Wang, H. L. *et al*. RecET direct cloning and Redab recombineering of biosynthetic gene clusters, large operons or single genes for heterologous expression. Nat. Protoc. **11**, 1175–1190 (2016).
23. Wang, H. L. *et al*. ExoCET: exonuclease invitroassembly combined with RecET recombination for highly efficient direct DNA cloning from complex genomes. Nucleic. Acids. Res. **46**, 5–16 (2018).
24. Bai, C. X. *et al*. Exploiting a precise design of universal synthetic modular regulatory elements to unlock the microbial natural products in *Streptomyces*. *Proc. Natl. Acad. Sci.* **112**, 12181–12186 (2015).
25. Gould, S. J. Cheng, X. and Halley, K. A. Biosynthesis of dehydrorabelomycin and PD 116740: prearomatic deoxygenation as evidence for different polyketide synthases in the formation of benz[a]anthraquinones. J. Am. Chem. Soc. **114**, 10066–10068 (1992).
26. Zhu, W. *et al*. Characterization of bioactivities and biosynthesis of angucycline/angucyclinone derivatives derived from *gephyromycinifex aptenodytis* gen. nov., sp. nov. Mar. Drugs, 20, 34–45 (2022).
27. Kharel, M. K., Pahari, P., Lian, H., Rohr, J. Enzymatic total synthesis of rabelomycin, an angucycline group antibiotic. Org. Lett. **12**, 2814–2817 (2010).

28. Kallio,P., Liu, Z., Mäntsälä, P., Niemi, J. and Metsä-Ketelä, M. Sequential action of two flavoenzymes, PgaE and PgaM, in angucycline biosynthesis: chemoenzymatic synthesis of gaudimycin C. Chem. Biol. **15**, 157–166 (2008).
29. Patrikainen, P. *et al*. Tailoring enzymes involved in the biosynthesis of angucyclines contain latent context-dependent catalytic activities. Chem. Biol. **19**, 647–655 (2012).
30. Liu, X. Y. *et al*. Heterologous biosynthesis of type II polyketide products using *E. coli*. ACS. Chem. Biol. **15**, 1177–1183 (2020).
31. Kim, K. Boyd, V. A. Sobti, A. Sulkowski, G. A. A unified strategy for the total synthesis of the angucycline antibiotics SF 2315A, Urdamycinone B, and the shunt metabolite 104-2. Isr. J. Chem. **37**, 3–22 (1997).
32. Yang, C. F. *et al*. Inactivation of flavoenzyme-encoding gene flsO1 in fluostatin biosynthesis leads to diversified angucyclinone derivatives. J. Org. Chem. **86**, 11019–11028 (2021).
33. Jumper, J. *et al*. Highly accurate protein structure prediction with AlphaFold. Nature **596**, 583–589 (2021).
34. Eberhardt, J., Santos-Martins, D., Tillack, A.F. and Forli, S. AutoDock vina 1.2.0: new docking methods, expanded force field, and python bindings. J. Chem. Inf. Model. **61**, 3891–3898 (2021).
35. Fu, J. *et al*. Full-length RecE enhances linear-linear homologous recombination and facilitates direct cloning for bioprospecting. Nat. Biotechnol. **30**, 440–446 (2012).
36. Liu, Y. *et al*. Discovery of polycyclic macrolide shuangdaolides by heterologous expression of a cryptic trans-AT PKS gene cluster.Org. Lett. **23**, 6967–6971 (2021).
37. Kieser, T. *et al*. Practical Streptomycetes Genetics, *The John Innes Foundation: Norwich*, UK, (2000).
38. Wang, H. *et al*. Improved seamless mutagenesis by recombineering using ccdB for counterselection. Nucleic. Acids. Res. **42**, e37-47 (2014).
39. Mosmann, T. Rapid colorimetric assay for cellular growth and survival: application to proliferation and cytotoxicity assays. J. Immunol. Methods, **65**, 55–63 (1983).
40. Skehan, P. *et al*. New colorimetric cytotoxicity assay for anticancer-drug screening. J. Natl. Cancer. Inst. **82**, 1107–1112 (1990).
41. Frisch, M. J. *et al*. Gaussian 09, revision D.01; Gaussian Inc.: Wallingford, CT. (2013).
42. Zhao, Y.; Truhlar, D. G. The M06 suite of density functionals for main group thermochemistry, thermochemical kinetics, noncovalent interactions, excited states, and transition elements: two new functionals and systematic testing of four M06-class functionals and 12 other functionals. Theor. Chem. Acc. **120**, 215–241(2008).
43. Cossi, M.; Rega, N.; Scalmani, G.; Barone, V. Energies, structures, and electronic properties of molecules in solution with the C-PCM solvation model. J. Comput. Chem. **24**, 669–681(2003).

Figures

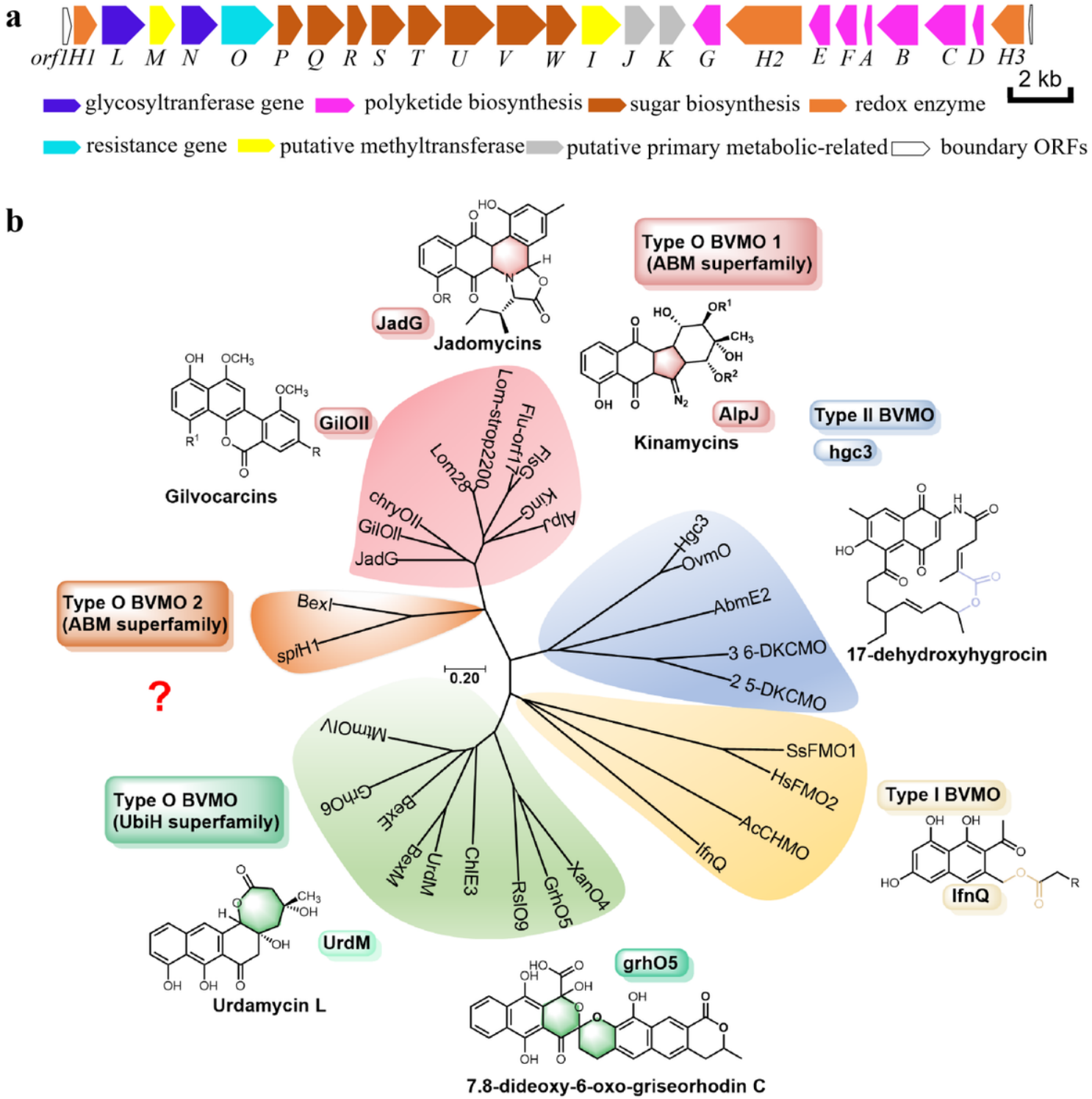

Figure 1

Genome mining on HDN155000 revealed the type II PKS *spi1* and the unique BVMO spiH1. a Organization of *spi1* BGC. **b** Phylogenetic analysis of *spi*H1 with other well-documented BVMOs. SpiH1 belongs to Type O BVMOs in the ABM superfamily. Structures highlights exemplify BVMOs catalytic specificity.

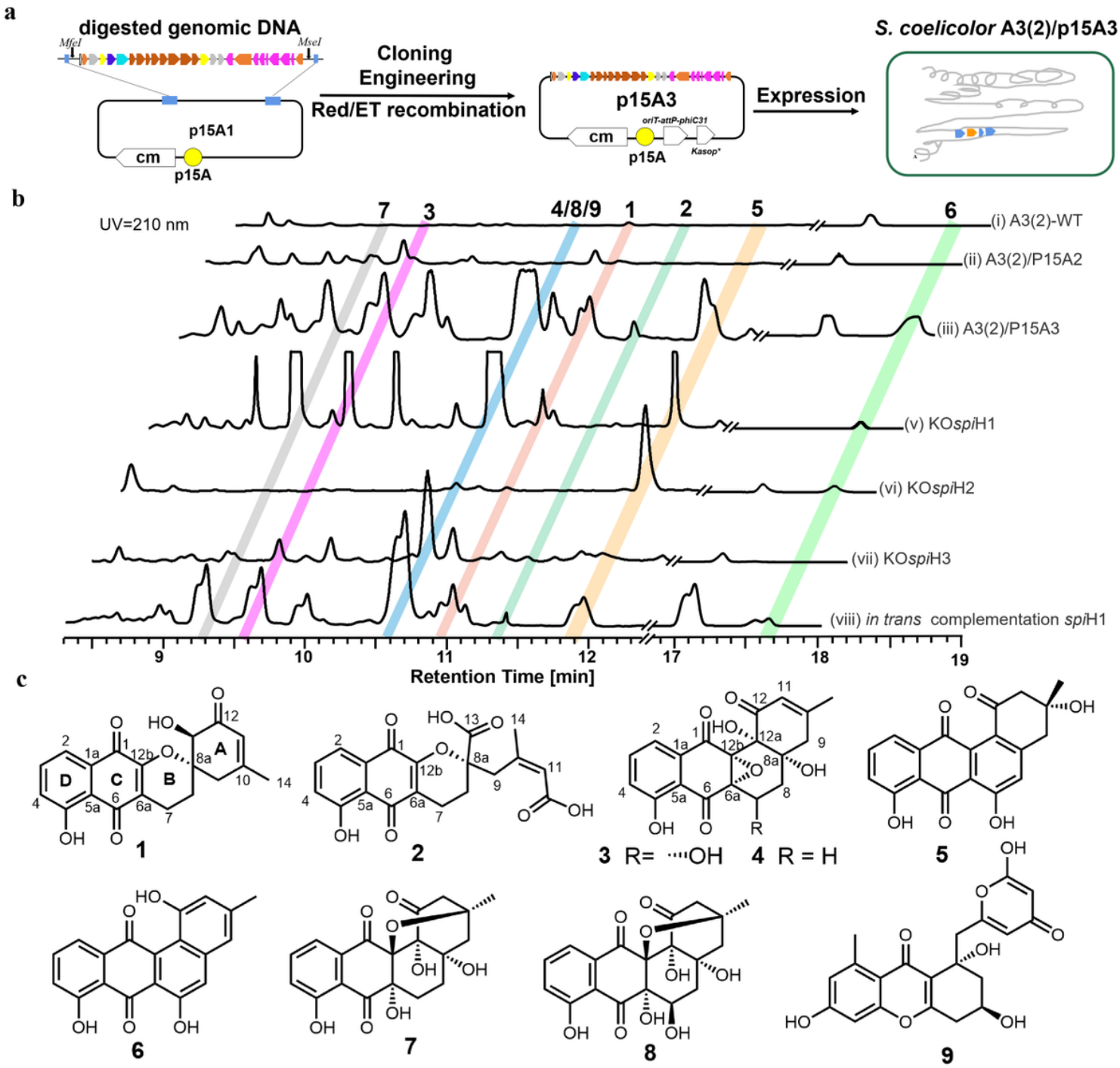

Figure 2

Direct cloning and heterologous expression of *spi1* BGC led to the discovery of novel spirocyclione derivatives. a The *spi1*cluster was directly cloned into p15A backbone by Red/ET recombineering and heterologously expessed in *S. coelicolor* A3(2). **b** HPLC-MS profile of *S. coelicolor* A3(2) harboring *spi1* BGC (iii) and mutational *spi1*BGC (v-vii) revealed the production of diversified angucycline products. **c**Structures obtained from heterologous expression of *spi1* BGC.

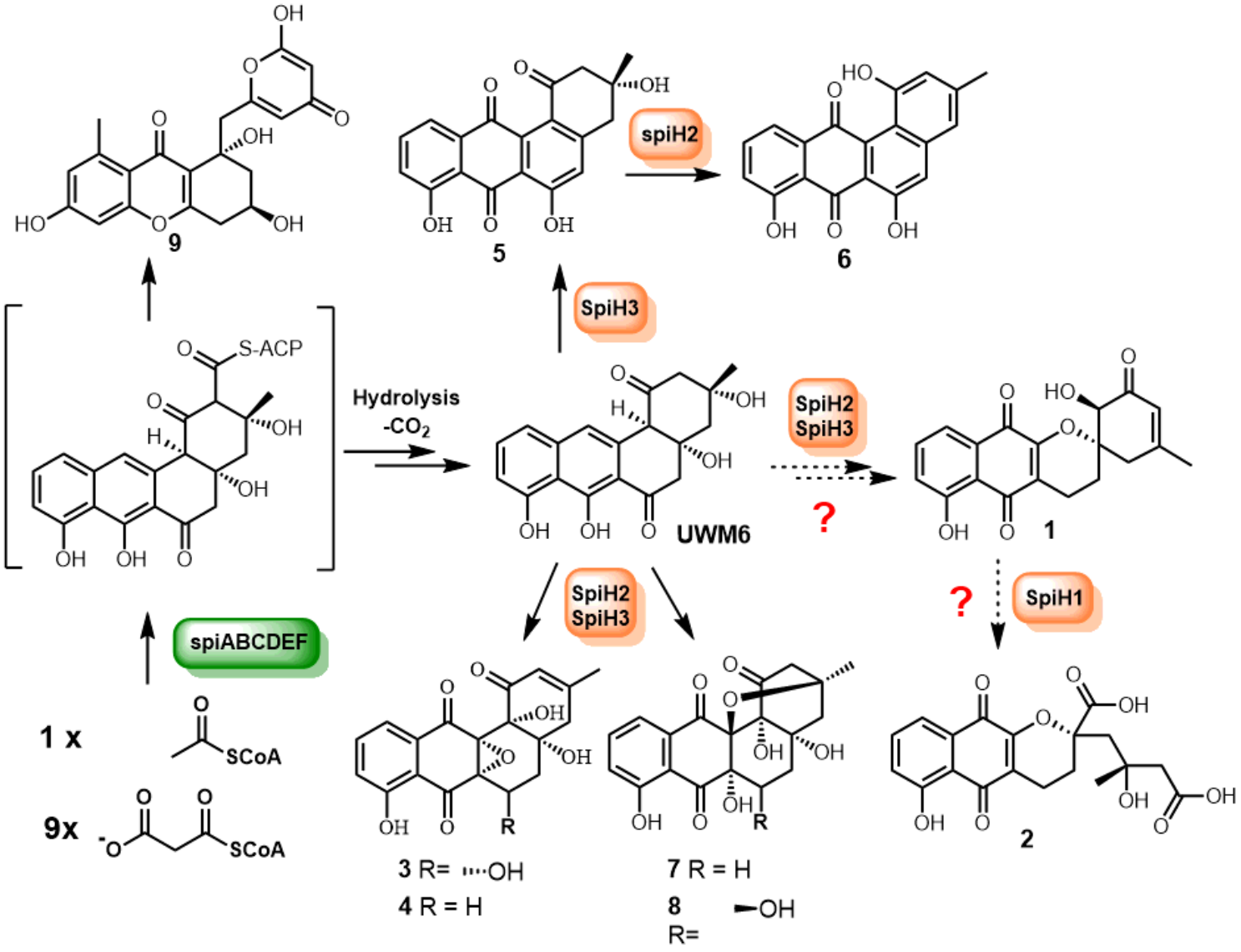

Figure 3

Proposed biosynthetic pathway leading to atypical angucyclines. Angyucycline derivatives are reported to share the early biosynthetic pathway starting from acetyl-CoA to the general intermediate of UWM6. Compounds **3**-**8** are presumed to be derived UMW6 catalyzed by SpiH2 and SpiH3. Further oxidative modifications catalysed by SpiH1 in addition to SpiH2 and SpiH3 are proposed to be responsible for the formation of compounds **1**-**2**.

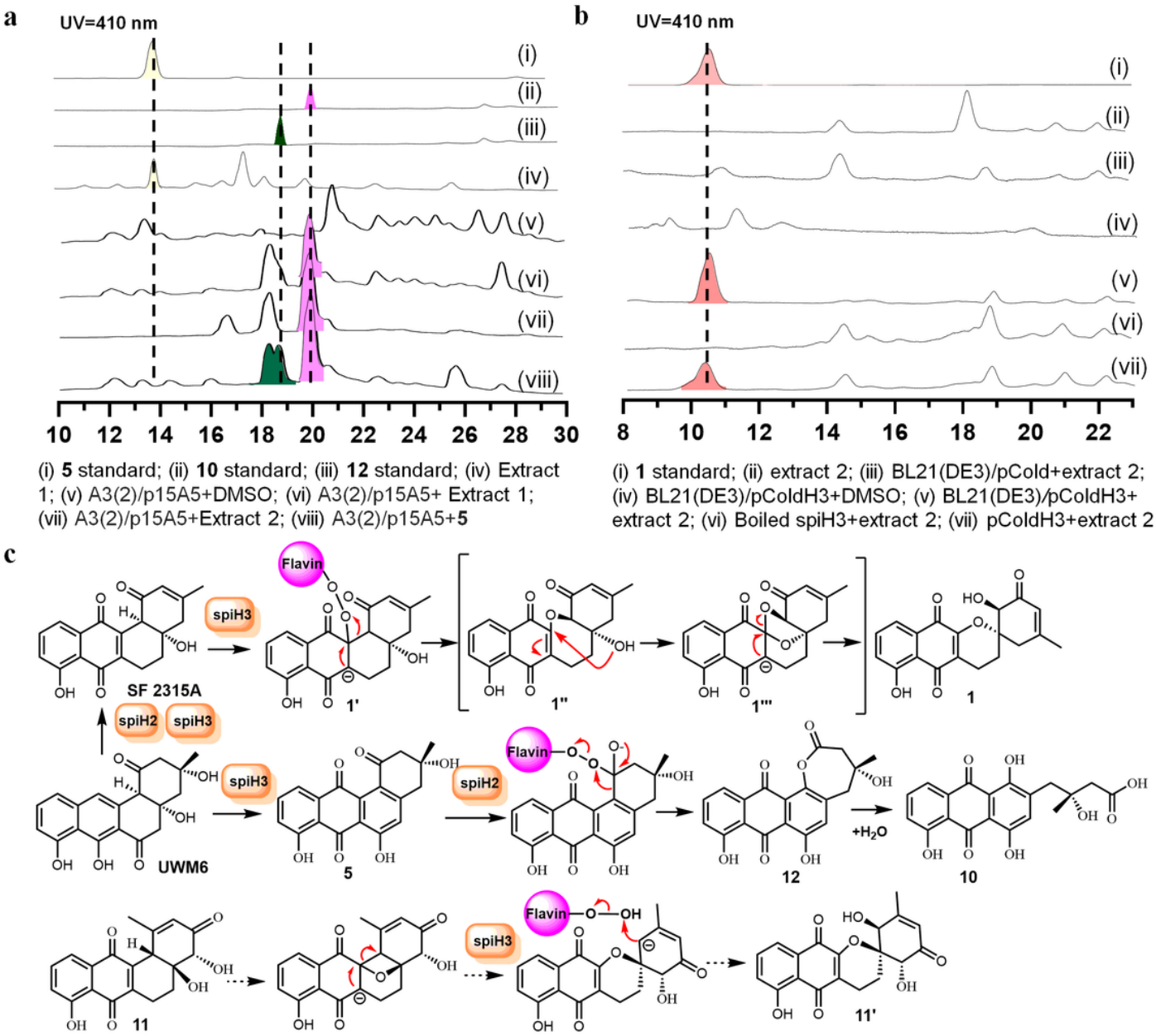

(i) **5** standard; (ii) **10** standard; (iii) **12** standard; (iv) Extract 1; (v) A3(2)/p15A5+DMSO; (vi) A3(2)/p15A5+ Extract 1; (vii) A3(2)/p15A5+Extract 2; (viii) A3(2)/p15A5+**5**

(i) **1** standard; (ii) extract 2; (iii) BL21(DE3)/pCold+extract 2; (iv) BL21(DE3)/pColdH3+DMSO; (v) BL21(DE3)/pColdH3+ extract 2; (vi) Boiled spiH3+extract 2; (vii) pColdH3+extract 2

Figure 4

Biosynthesis of Spirocyclione A (1). a HPLC analysis of extract from *S. coelicolor* A3(2)/p15A5 fed with early angular intermediates. **b** *In vivo* and *in vitro* biotransformation of early angular intermediates by SpiH3 produced from *E. coli* BL21(DE3). **c** Proposed biosynthetic pathway from UWM6 to **1**.

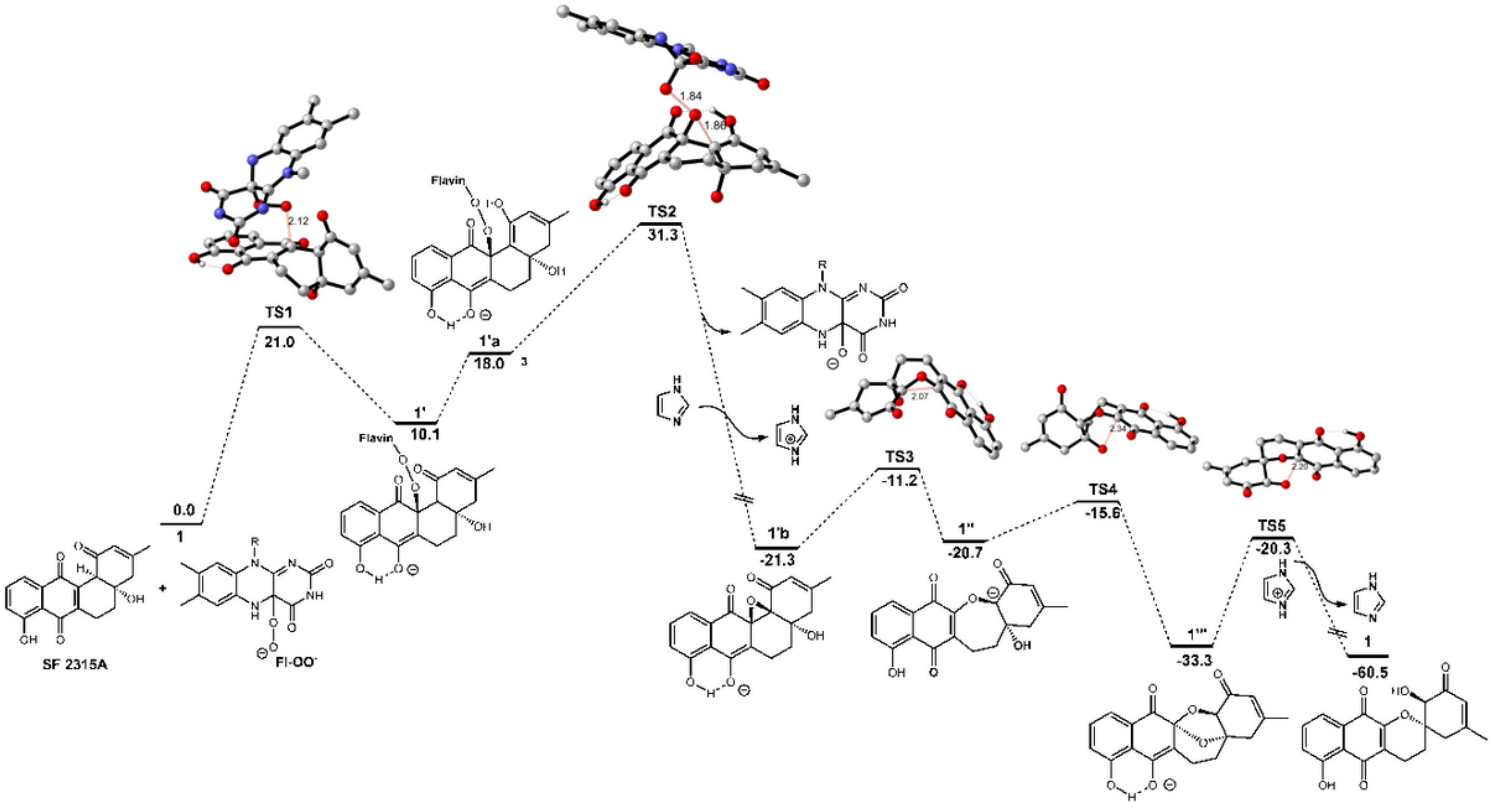

Figure 5

DFT calculation of Gibbs free energies (in kcal mol-1) at the CPCM(water)-M06-2X/6–311+G(d,p)//CPCM(water)-M06-2X/6–31G(d) level of theory and the computed transition-state structures (Hydrogen: omit, carbon: grey, Oxygen: red, Nitrogen: blue, and distances are shown in Å).

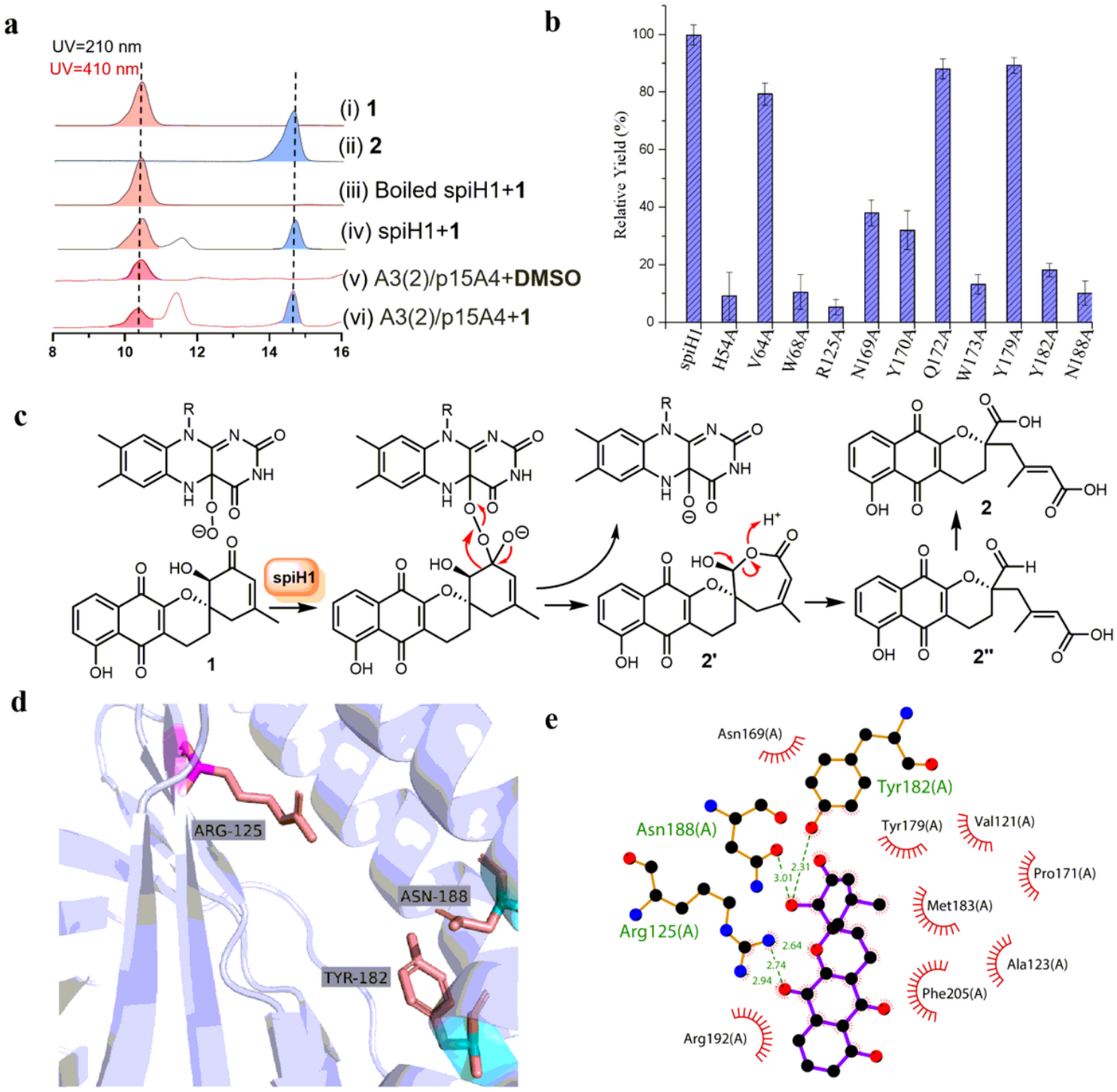

Figure 6

Functional characterization of SpiH1. a LC-MS analysis of SpiH1 catalysed reaction in the presence of NADPH, FAD and Fre. **b**Biotransformation from **1** to **2** catalysed by SpiH1. **c**Relative specific activities of SpiH1 mutants. **d** The C-terminal hydrophobic pocket and the predicted best binding conformation for **1**. **e**LigPlot+ representation of the binding mode for **1** in the putative C-terminal active sites of SpiH1.

Supplementary Files

This is a list of supplementary files associated with this preprint. Click to download.

- SupportingInformation0915.docx